Available online at www.sciencedirect.com
ScienceDirect
Geochimica et Cosmochimica Acta 70 (2006) 4783–4796
Geochimica
www.elsevier.com/locate/gca

A geochemical approach to model periodically replenished magma chambers: Does oscillatory supply account for the magmatic evolution of EPR 17–19°S?

Eric Rannou [a,*], Martial Caroff [b], Carole Cordier [b]

[a] *UMR No 6205 "Laboratoire de Mathématiques," Université de Bretagne Occidentale, 6 Avenue Le Gorgeu, C.S. 93837, 29238 Brest Cedex 3, France*
[b] *UMR No 6538 "Domaines Océaniques," IUEM, Université de Bretagne Occidentale, 6 Avenue Le Gorgeu, C.S. 93837, 29238 Brest Cedex 3, France*

Received 21 November 2005; accepted in revised form 6 July 2006

Abstract

We propose a new approach to model the geochemical evolution of continuously replenished and tapped steady-state magma chambers. We use a sinusoidal function to model cyclic magma supply. The temporal evolution of a reservoir is described using differential equations, in which the amount of refilling magma does not depend on the size of the chamber. These equations can be used to calculate incompatible trace element concentrations and magma quantities. We examine the geochemical consequences of episodic injections, noises and wall-rock assimilation. We also explore possible variations in crystallization rate. To show its potential, the theoretical treatment has been applied to the EPR 17–19°S, a site with a strong magma budget which has been the subject of several geological/geophysical studies. The practical application requires geological parameters to be constrained, as well as the extreme values of the lava concentration range. A first step specifies the incompatible trace element composition of the replenishing melt, which corresponds in the EPR case to a magnesian liquid (MgO = 9.5 wt%). It is then possible to determine other parameters such as cycle period (~750 years), magma residence time (~300 years), and reservoir size (from 4.1 to 8.6 km^3 per 20 km segment). Lastly, variations in crystallization rate do not significantly alter the results.

1. Introduction

The linkage between energetics and material balances in the magmatic systems can be numerically treated either through geochemical models which formalize physical processes (e.g., Ghiorso and Sack, 1995; Edwards and Russell, 1998; Spera and Bohrson, 2002, 2004) or though mass balance models in which physics is not directly apparent, but enclosed into a few integrative parameters.

In the physicochemical models, the modeling exercise appeals directly to physical laws in order to address complex natural systems. However such modeling processes must make use of a great number of input parameters, the values of which are not highly constrained. For instance, to model instantaneous heat transfer in a magma chamber, heat loss to country rocks (roughly proportional to the surface area of the reservoir) must be taken into account together with the effects of thermal and/or solutal convection, replenishment by hot liquids, wall-rock assimilation, etc. In such an approach, the realism of the method is counterbalanced by the difficulty to obtain a set of useful output parameters.

Alternatively, there are models based on integrative methods, which can be used to reduce the number of parameters and make their estimation easier without too much simplification.

Two kinds of integrative procedures have been developed for modeling the behavior of replenished magma reservoirs from geochemical data (see Caroff and Fleutelot, 2003, for a review). The first group uses mass balance calculations to explore trace element variations in long-lived

* Corresponding author. Fax: +33 298016790.
E-mail address: Eric.Rannou@univ-brest.fr (E. Rannou).

0016-7037/$ - see front matter © 2006 Elsevier Inc. All rights reserved.
doi:10.1016/j.gca.2006.07.007

periodically replenished, periodically tapped and continuously fractionating steady-state magma chambers (O'Hara, 1977; Albarède, 1985; O'Hara and Herzberg, 2002). The second set of theoretical treatments applies to continuously replenished, (occasionally or) continuously tapped and continuously fractionating magma chambers (De Paolo, 1981; Reagan et al., 1987; Caroff et al., 1997). Contrary to the former models, such approaches are used to track instantaneous geochemical evolutions, using differential equations.

Caroff et al. (1997) studied the case where both magma refilling and expulsion are simultaneous and continuous processes at the geological time scale. In such reservoirs, the total amount of liquid either decreases (deflating chambers) or increases (inflating chambers) through time. These authors have shown that the geochemical differentiation of the erupted lavas is strongly controlled by the mass fluxes through the system. The corresponding model had been applied to four segments of the East Pacific Rise located between 17°00′S and 18°40′S.

The modeling by Caroff et al. (1997) includes several simplifying assumptions: (i) each stage of evolution of the reservoir (i.e. deflating or inflating phase) was studied separately; (ii) the crystallization rate was assumed to be constant between the two stages; and (iii) all the magma fluxes (replenishment, expulsion, and crystallization) were fixed proportional to the reservoir size.

We propose here a new numerical approach to avoid some limitations of the Caroff et al. (1997) model, while retaining its ability to calculate at little cost geologically significant parameters from specific geological constraints. The main improvement introduced here is that the amount of refilling magma is not dependent on the chamber size. However, the characteristics of the magma supply ultimately control the temporal evolution of the reservoir. Among the various modalities of replenishment which can be modeled, including constant magma flux, we have chosen to consider a sinusoidal form of replenishment. Such a mathematical function has been used successfully by Albarède (1993) to model periodic chemical fluctuations in magmas passing through a constant size reservoir. Our approach allows us temporal periodicity of the magmatic system to be explored through differential equations and reconciles both concepts about the open-system magma chambers: periodic and continuous inputs.

A great part of the compositional variations described for oceanic/ophiolitic cumulates and lavas has been interpreted as the consequence of periodic intrusions of magma into axial reservoirs beneath spreading ridges (e.g., Pallister and Hopson, 1981; Smewing, 1981; Komor et al., 1985; Humler and Whitechurch, 1988; Caroff and Fleutelot, 2003). The temporal cyclicity of magma supply can be related to fluctuations in the magma delivery from the oceanic mantle. Such fluctuations can result from periodic magma pulses at the surface (Maaløe, 2002), modeled as 'magma solitons' by some authors (Scott and Stevenson, 1984; Rabinowicz et al., 2001). In anhydrous basaltic reservoirs, expulsion of magma is not likely to lead to gas-driven catastrophic events such as those which occur in arc settings. Consequently, time-related magma expulsion beneath spreading ridges should be more easily modeled. In an accretion context, wall-rock assimilation is supposed to play a subordinate role with respect to fractional crystallization. We have reinvestigated the geological site (EPR 17–19°S) previously studied by Caroff et al. (1997). In this zone, known for its strong magma budget (e.g., Carbotte et al., 1997; Hussenoeder et al., 2002), the variable across-strike ridge profile is a sensitive indicator of a cyclic magma supply (Lagabrielle and Cormier, 1999). Thus, the configuration of this site is particularly adequate for the application of our new geochemical approach. The trace element data set of Caroff et al. (1997) has been extended to include additional published analyses.

Among the output parameters, we are capable of estimating cycle periods and magma residence times. Few measurements of such temporal data are presently available for submarine volcanic zones, in order to make a comparison with calculated parameters, contrary to the case of well studied replenished continental volcanoes (e.g., Hawkesworth et al., 2000). Nevertheless, we have chosen not to apply the present procedure to continental volcanoes, where: (i) steady-state can be considered as an exceptional feature (e.g., Cioni et al., 1995), (ii) assimilation is generally drastic (e.g., Kabeto et al., 2001), (iii) differentiation has frequently a much greater extent, which may induce magma stratification and imperfect mixing processes (e.g., Cioni et al., 1995).

The present procedure includes two parts : (i) a purely theoretical development, potentially applicable to magmatic systems from various geological settings; and (ii) a practical application specifically adapted to the case of EPR 17–19°S. The first and less constraining-step of the modeling, which consists to calculate incompatible trace element composition of the replenishment liquid, has also been tested on another oceanic site: the north-south propagating spreading center located in the North Fiji Basin between 18 and 19°S (NS-PSC 18–19°S). Such applied modelings must be modulated according to the level of geological knowledge of the studied sites. The precision of the output data (geochemical, temporal, or mass-related parameters) is highly dependent on the accessibility and reliability of the input parameters.

2. Fluctuating replenishment in continuously fractionated and tapped magma chambers

2.1. Theory

In the model proposed here, the magma chamber behavior is studied through the time variation of the resident magma quantity Q. Let Q_i, Q_c, and Q_e be the time integrated quantities of injected, crystallized and expelled magmas, respectively (see Table 1 for definition of the model parameters). The resident magma quantity Q satisfies the following differential equation:

Table 1
Model parameters

Quantities[a]	
Q	Quantity of resident magma in the reservoir
Q_0	Initial quantity of resident magma in the reservoir
Q_e	Quantity of expelled magma
Q_c	Quantity of crystallized magma
Q_i	Quantity of injected magma
q_i	Instantaneous rate of intrusion: $q_i = \frac{dQ_i}{dt}$
$\overline{q}_i$	Mean rate of intrusion
a	Quantity of magma crystallizing per time unit fixed independently of Q
Chemical parameters	
Q^E	Quantity of an incompatible trace element E in the resident magma
C_i^E	Weight concentration of an incompatible trace element E in the injected magma (ppm)
C^E	Weight concentration of an incompatible trace element E in the resident magma (ppm): $C^E = \frac{Q^E}{Q}$
D^E	Bulk distribution coefficient of an incompatible trace element E
Fractions	
α	Fraction crystallized per time unit: $\alpha = \frac{1}{Q}\frac{dQ_c}{dt}$
α_p	Fraction crystallized per time unit (part dependent on Q in the non-proportional approach)
r_e	Mean ratio between extrusion rate and crystallization rate: $r_e = \frac{dQ_e}{dQ_c}$
γ	Fraction of magma lost by crystallization and extrusion per time unit: $\gamma = \alpha(1 + r_e)$
γ_p	$\gamma_p = \alpha_p(1 + r_e)$
γ^E	Fraction of trace element E lost by crystallization and extrusion: $\gamma^E = \alpha(D^E + r_e)$
γ_p^E	$\gamma_p^E = \alpha_p(D^E + r_e)$
Sinusoidal model parameters	
$\omega/(2\pi)$	Frequency of the replenishment
T	Period of the replenishment: $T = 2\pi/\omega$
φ	Phase shift between variations of Q and q_i: $\varphi = -\arcsin\frac{\omega}{\sqrt{\omega^2+\gamma^2}} = -\arcsin\frac{\beta}{\sqrt{\beta^2+(1+r_e)^2}}$
φ^E	Phase shift between variations of Q^E and q_i: $\varphi^E = -\arcsin\frac{\omega}{\sqrt{\omega^2+\gamma^{E2}}} = -\arcsin\frac{\beta}{\sqrt{\beta^2+(D^E+r_e)^2}}$
β	$\beta = \omega/\alpha$
τ	Residence time: $\tau = 1/\gamma$

[a] The model has been expressed with magma masses and weight concentrations. However, the Q parameters can be easily transformed into magma volumes by introducing density values.

$$\frac{dQ}{dt} = \frac{dQ_i}{dt} - \left(\frac{dQ_c}{dt} + \frac{dQ_e}{dt}\right). \quad (1)$$

Like previous theoretical treatments (e.g., O'Hara, 1977; De Paolo, 1981; Reagan et al., 1987; O'Hara and Herzberg, 2002), our model is based on the simplifying assumption of proportionality between Q and the crystallized and expelled magma rates, respectively:

$$\frac{dQ_c}{dt} = \alpha Q \quad (2)$$

and

$$\frac{dQ_e}{dt} = \alpha r_e Q, \quad (3)$$

where α is the crystallized fraction per time unit and r_e the mean ratio between extrusion and crystallization rates. The total proportionality factor is $\gamma = \alpha(1 + r_e)$ (Table 1).

In the Caroff et al. (1997) model, the instantaneous rate of magma intrusion q_i is also considered proportional to Q (Table 1). During magma chamber growth, this assumption leads to an exponential inflation of the chamber. In the present model, q_i is strictly independent of Q. This implies that the characteristics of the processes occurring (or originating) inside the reservoir (crystallization, extrusion) are closely dependent on the intrusion process. Thus, the instantaneous rate of intrusion q_i is only time dependent: $\frac{dQ_i}{dt}(t) = q_i(t)$. Eq. (1) becomes then:

$$\frac{dQ}{dt} = q_i - \gamma Q, \quad (4)$$

the solution of which is

$$Q(t) = \left(Q_0 + \int_0^t q_i(x)e^{\gamma x}dx\right).e^{-\gamma t}, \quad (5)$$

where x is an integration parameter.

The simplest case which can be considered is when q_i is constant. Then, the magma quantity becomes:

$$Q(t) = \frac{q_i}{\gamma} + \left(Q_0 - \frac{q_i}{\gamma}\right).e^{-\gamma t}. \quad (6)$$

This solution leads exponentially to a steady state Q value equal to $\frac{q_i}{\gamma}$ (Fig. 1a).

We have also considered a geologically more realistic mode of intrusion, the sinusoidal one. The advantage of such an approach to model natural periodic systems is that it may approximate an average behavior or a smoothed variation with time. In this case, q_i and Q can be written, respectively:

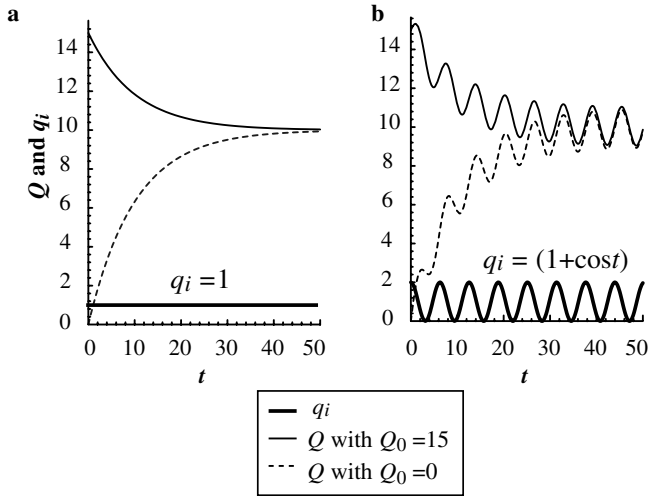

Fig. 1. Consequences of constant (a) and sinusoidal (b) intrusions on temporal variations of the resident magma quantity Q, calculated from Eqs. (6) and (8), respectively. In each diagram, two alternative initial situations of the reservoir (empty or containing an arbitrary quantity of magma) are considered. Q is calculated with $\gamma = 0.1$. Magma reservoirs tend exponentially toward a steady state behavior.

$$q_i(t) = \overline{q}_i(1 + \cos(\omega t)) \tag{7}$$

and

$$Q(t) = \frac{\overline{q}_i}{\gamma} + \frac{\overline{q}_i}{\sqrt{\gamma^2 + \omega^2}} \cos(\omega t + \varphi) + \left(Q_0 - \frac{\overline{q}_i}{\gamma}\left(1 + \frac{\gamma^2}{\gamma^2 + \omega^2}\right)\right).\mathrm{e}^{-\gamma t}, \tag{8}$$

where $\overline{q}_i$ is the mean rate of intrusion and φ is the phase shift. This latter parameter expresses the delay of the reservoir response in terms of size to the magma intrusion.

This solution leads exponentially to a magma quantity equal to the following steady state sinusoid function:

$$Q(t) = \frac{\overline{q}_i}{\gamma} + \frac{\overline{q}_i}{\sqrt{\gamma^2 + \omega^2}} \cos(\omega t + \varphi). \tag{9}$$

This quantity oscillates around a mean value $\overline{q}_i/\gamma$, with an amplitude of $2\overline{q}_i/\sqrt{\gamma^2 + \omega^2}$. The period $T = 2\pi/\omega$ of the function Eq. (9) is similar to that of the intrusion Eq. (7), but with a phase shift of φ (Fig. 1b).

Such an equation can be used to compute the residence time τ which can be defined as the ratio between the mean quantity of resident magma and the mean rate of injected magma:

$$\tau = \frac{\frac{1}{T}\int_0^T Q(t)\mathrm{d}t}{\frac{1}{T}\int_0^T q_i(t)\mathrm{d}t} = \frac{\frac{\overline{q}_i}{\gamma}}{\overline{q}_i} = \frac{1}{\gamma}. \tag{10}$$

Thus τ and γ are here inverse parameters.

2.2. Geochemical formulation

Our approach can be applied to any quantity fitting an equation of type (4), such as elemental weight concentrations. Incompatible trace elements (E) are especially suitable for such a modeling. The behavior of major elements and compatible trace elements is too much dependent on both the nature and the proportion of the fractionating minerals. In the geochemical approach, contributions of crystallization and extrusion must be separated inside the γ^{E} parameter, equal to $\alpha(D^{\mathrm{E}} + r_e)$, where D^{E} is the bulk distribution coefficient (Table 1). C_i^{E} is the concentration of an element E in the injected magma. Assuming that this parameter is constant, the quantity of E in the resident magma is

$$Q^{\mathrm{E}}(t) = \frac{C_i^{\mathrm{E}}\overline{q}_i}{\gamma^{\mathrm{E}}} + \frac{C_i^{\mathrm{E}}\overline{q}_i}{\sqrt{\gamma^{\mathrm{E}2} + \omega^2}} \cos(\omega t + \varphi^{\mathrm{E}}) + \left(Q_0^{\mathrm{E}} - \frac{C_i^{\mathrm{E}}\overline{q}_i}{\gamma^{\mathrm{E}}}\left(1 + \frac{\gamma^{\mathrm{E}2}}{\gamma^{\mathrm{E}2} + \omega^2}\right)\right).\mathrm{e}^{-\gamma^{\mathrm{E}} t}. \tag{11}$$

Combining Eqs. (8) and (11) allows us to obtain the function $C^{\mathrm{E}} = Q^{\mathrm{E}}/Q$, which leads exponentially to a steady state C^{E} value equal to:

$$C^{\mathrm{E}}(t) = C_i^{\mathrm{E}} \frac{\frac{1}{\gamma^{\mathrm{E}}} + \frac{\cos(\omega t + \varphi^{\mathrm{E}})}{\sqrt{\gamma^{\mathrm{E}2} + \omega^2}}}{\frac{1}{\gamma} + \frac{\cos(\omega t + \varphi)}{\sqrt{\gamma^2 + \omega^2}}} = C_i^{\mathrm{E}} \frac{\frac{1}{D^{\mathrm{E}} + r_e} + \frac{\cos(\omega t + \varphi^{\mathrm{E}})}{\sqrt{(D^{\mathrm{E}} + r_e)^2 + \beta^2}}}{\frac{1}{1 + r_e} + \frac{\cos(\omega t + \varphi)}{\sqrt{(1 + r_e)^2 + \beta^2}}}. \tag{12}$$

C^{E} is proportional to C_i^{E} (assumed to be a constant) and the amplitude of its variations strongly depends on parameter β, defined as the ratio between ω (frequency multiplied by 2π) and crystallization rate α, also assumed to be a constant (Table 1). Consequently, once the other parameters are estimated, it is possible to determine C_i^{E} and β only from the maximum and minimum values of C^{E} (measured in the lavas).

2.3. Properties of the model

2.3.1. Low versus high frequencies

Our procedure belongs to a group of geochemical models widely used in several scopes: e.g., hydrogeology, sedimentology, and magmatology. The linearity of the differential equations is a mathematical property which simplifies the expression of natural systems. For example, linearity can be used to study the behavior of a magma chamber only through the total input flux, even if the reservoir is filled from several feeder zones.

From a mathematical point of view, elementary functions (here sinusoids) can be added together, as a consequence of the linearity, in order to obtain new functions. Through Fourier's decompositions, any periodic intrusion function can be split into sinusoids.

In other respects, because the amplitude of Q (Eq. (9)) and Q^{E} increases when the frequency decreases, low frequencies are amplified more. For example, in Fig. 2

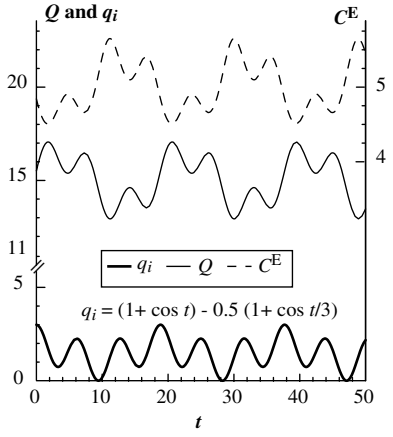

Fig. 2. Consequences of a strong perturbation of the intrusion signal on resident magma quantity Q and on concentrations C^{E}, for a steady-state magma reservoir. Q and C^{E} functions are calculated from Eqs. (9) and (12), respectively. The input signal is the sum of two functions, the amplitudes and periods of which are different. γ and γ^{E} are taken equal to 0.1 and 0.02, respectively, and C_i^{E} to 1.

the linearity properties allow illustration of the consequences of an intrusion which is the sum of two different sinusoidal functions. In contrast with the input signal, the component with the shortest period is strongly attenuated in the output signals.

2.3.2. Noises

It is unlikely that periodic replenishments follow accurately a sinusoidal function. Consequently, we propose to examine the effects of large disturbances in an input q_i sinusoid (considered as reference in the next sections). Let us consider, as previously, the sum of two sinusoidal functions having contrasted periods, then apply random fluctuations to their amplitudes. Summing two sinusoids (one subordinate with respect to the other) is used here to generate disturbances which are not coeval with the main reference sinusoid. We have chosen a set of input parameters close to those which will be discussed later in the text, in the EPR section. Results are shown in Fig. 3a. Noises in the input signal have very slight repercussions on the shape of the output concentration curve for the highly incompatible element E. The extreme values are very close to those of the reference output signal. Noises behave like a high-frequency signal, attenuated by the magmatic system.

Consequently, the model is robust to noises and other discontinuities of natural systems, since it amplifies the signals which are geologically significant.

2.3.3. Chemical outcome of a noise-corrupted model derived from O'Hara (1977)

O'Hara (1977) has proposed a periodical model in which the resident magma differentiates for a long time in closed-system reservoirs between two short-lasting refilling episodes. At steady state, this type of replenishment can be represented through a periodical crenelated q_i curve, showing narrow and high peaks separated by long stages of quietness. The corresponding signal is shown in Fig. 3b together with a reference input sinusoid, similar parameters being used in both cases. Supposing the ejection is continuous (in contrast with the O'Hara's model), the response of the magma chamber in terms of incompatible element concentrations is a dissymmetrical periodic curve, with a maximum concentration value higher than for the reference sinusoidal model. A noisy O'Hara-type signal, also shown in Fig. 3b, has been constructed by distributing the $\overline{q}_i$ value (0.02 km^3/year) into peaks (78%) and noises (22%). We obtain also a dissymmetrical concentration curve as result, but in this case the peak value is much closer to the maximum reference value. Thus, from a geochemical point of view, a noisy model derived from O'Hara (1977) tends to give output data close to those obtained through a pure sinusoidal model.

2.3.4. Assimilation effects on melt chemistry

In a magmatic system with a strong magma budget, even if wall-rock assimilation occurs, mass balance of trace elements is thought to be mainly controlled by the uncontamined magma. We propose to examine here the effects of wall-rock assimilation on the concentration of a highly incompatible element like Ce (D^{Ce} taken equal to 0.01) in the specific case of oceanic ridge reservoirs, settled within gabbroic surroundings. We have supposed that the roof of the magma chamber undergoes partial melting to

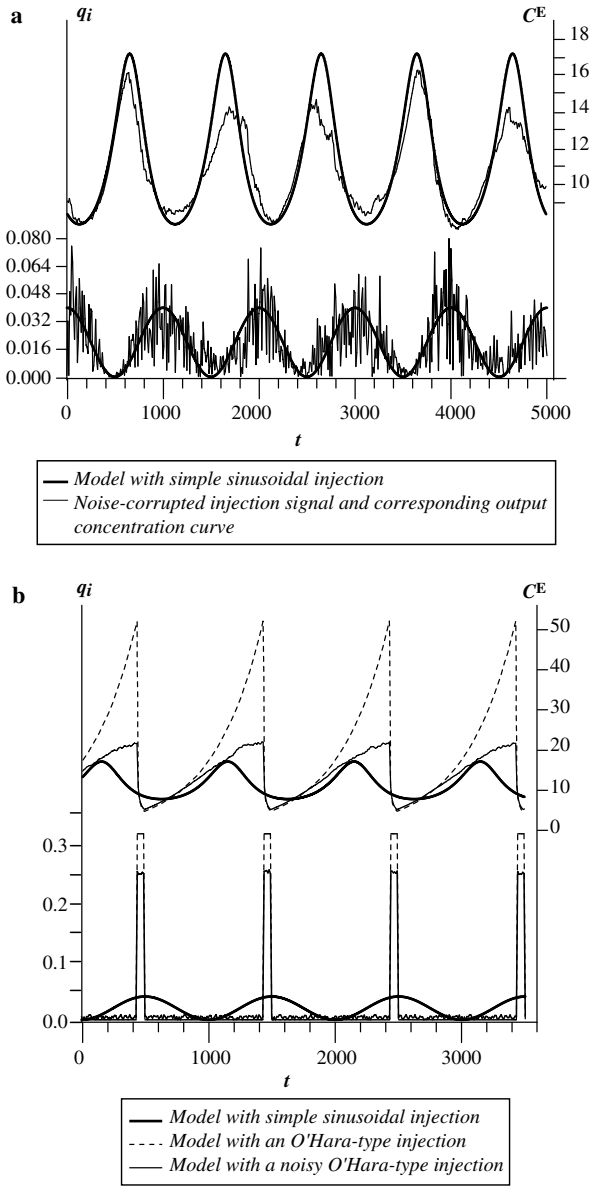

Fig. 3. Consequences of perturbations in the intrusion signal. The input parameter values are: 0.02 km^3/year for $\overline{q}_i$ (mean rate of intrusion); 1000 years for the period T; $D^E = 0.01$; 25×10^{-4} year^{-1} for α (fraction crystallized per unit time); and 0.4 for r_e (mean ratio between extrusion and crystallization rates). The zero value of time t is arbitrary. (a) Consequences of noises. Random fluctuations are applied every 10 years to the input signal, corresponding to the sum of two sinusoids. Noises have slight repercussions on the output incompatible element concentrations. (b) Discontinuous replenishment with narrow and high peaks separated by long stages of quietness, like in the O'Hara's (1977) model. The response of the reservoir in terms of incompatible element concentration is a dissymetrical periodic curve, with a maximum value close to that obtained with a sinusoidal model as soon as the discontinuous input signal is corrupted by noises. See text for more explanations.

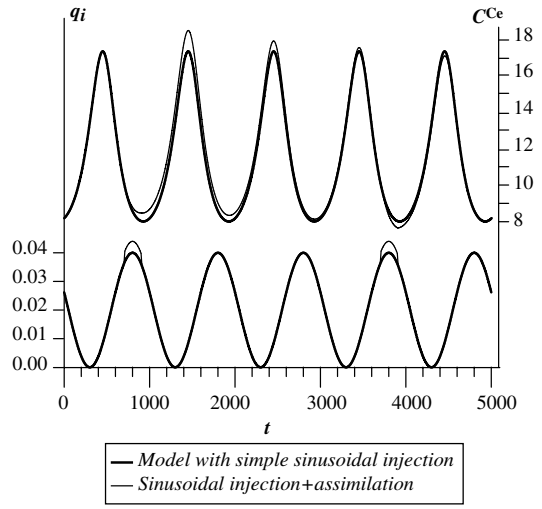

Fig. 4. Assimilation tests. Input parameters as in Fig. 3. We propose the assimilation during 200 years of two kinds of wall-rocks, corresponding to a quantity of 10% of the incoming magma: a leucosome vein with 12 ppm Ce between $t = 700$ and $t = 900$ years and a gabbro with 1 ppm Ce between $t = 3700$ and $t = 3900$ years. The difference in output Ce concentrations does not exceed 7% with respect to the assimilation-free model.

form anatectic migmatites, as suggested by Gillis and Coogan (2002). In our assimilation test (using a set of parameters similar to the noise test), the refilling magma has a Ce content of 3 ppm. The magmatic system assimilates a quantity of rocks corresponding to 10% of the incoming liquid during 200 years (i.e. a fifth of period) when the refilling rate is maximal. Two events are considered in Fig. 4: the first one corresponds to the assimilation of a leucosome vein with 12 ppm of Ce and the second one, to the assimilation of a REE-poor gabbro bearing 1 ppm of Ce (data from Gillis and Coogan, 2002). The curve of Ce in the contaminated magma appears to be slightly modified with respect to the reference output curve. The leucosome assimilation leads to a peak increasing from 17.2 to 18.3 ppm just after the event, then to a damped value of 17.8 ppm at the following cycle. The gabbro assimilation results in a barely perceptible depletion in the following valley (7.5 ppm instead of 7.9 ppm without assimilation).

2.4. Breaking the strict proportional relationships

Until now, our theoretical approach has been based on the simple assumption, already made by Caroff et al. (1997), that the crystallization $\alpha = \frac{1}{Q}\frac{\mathrm{d}Q_c}{\mathrm{d}t}$ and extrusion $\frac{1}{Q}\frac{\mathrm{d}Q_e}{\mathrm{d}t}$ fractions remain constant. However, thermal constraints are thought to vary as a function of the reservoir size. Indeed, the temperature gradient is highly dependent on hydrothermal and conductive cooling together with advection of heat from melt supply. Thus, the parameter α (Table 1) is likely to vary when the reservoir size is decreasing. To account for this geological constraint, let us assume a crystallization rate a independent of Q. Then, α becomes time-dependent and can be written:

$$\alpha(t) = \alpha_p + \frac{a}{Q(t)} \tag{13}$$

in which α_p is the constant component, corresponding to the previous α value.

Previous comparable models (Reagan et al., 1987; Caroff et al., 1997) have postulated a constant ratio r_e between extrusion and crystallization rates. If we adopt this view, $\frac{\mathrm{d}Q_e}{\mathrm{d}t}(t) = r_e\alpha(t)Q(t)$. Then, Eq. (1) becomes:

$$\frac{\mathrm{d}Q}{\mathrm{d}t} = q_i - a\frac{\gamma_p}{\alpha_p} - \gamma_p Q \tag{14}$$

which corresponds mathematically to Eq. (4) with an intrusion rate equal to $q_i - a\frac{\gamma_p}{\alpha_p}$ instead of q_i.

Regarding the formulation of Q^{E}, Eq. (1) expressed with $\gamma_p^{\mathrm{E}} = \alpha_p(D^{\mathrm{E}} + r_e)$ becomes

$$\frac{\mathrm{d}Q^{\mathrm{E}}}{\mathrm{d}t} = C_i^{\mathrm{E}}q_i - \gamma_p^{\mathrm{E}}\left(1 + \frac{a}{\alpha_p Q}\right)Q^{\mathrm{E}}. \tag{15}$$

This equation is not of the same type as Eq. (4). Through the numerical behavior of the corresponding solutions, it is possible to investigate the effects of variations in the rates of crystallization and extrusion.

3. East pacific rise from 17°S to 19°S

3.1. Large summit troughs as a reflection of variable reservoir states?

The axial volcanic zone of the east pacific rise (EPR) exhibits two kinds of morphology: broad, shallow, dome-shaped portions (commonly midsections of first-order ridge segments) and narrow, deep, triangular portions (generally ends of first-order segments). Seismic reflection studies have shown that a horizon marking the magma lens at the top of the axial magma chamber (AMC), present along more than 60% of the EPR, is typically detected beneath the dome-shaped regions (Detrick et al., 1987). This along-axis morphological variability has been attributed to differences in magma supply, with highest magma budget associated with dome-shaped ridge portions (Hooft et al., 1997).

The EPR between 16°30′S and 19°03′S is part of a 1150 km-long first order segment located between the Garrett transform and Easter microplate, and only interrupted by nontransform offsets (Fig. 5a). The spreading rate there is close to the fastest observed at the present time on Earth (ca. 150 mm/yr, DeMets et al., 1990). The corresponding axis is systematically dome-shaped. Three overlapping spreading centers (OSC) define, from south to north, the four second-order segments H, I, J, and K (Fig. 5b). Each of them displays a specific axial morphology: segment K axis has a typically smooth morphology whereas the three other ones are notched by more or less wide troughs (>500 m). Very recent volcanic activity has occurred along the axis in each segment (Auzende et al., 1996).

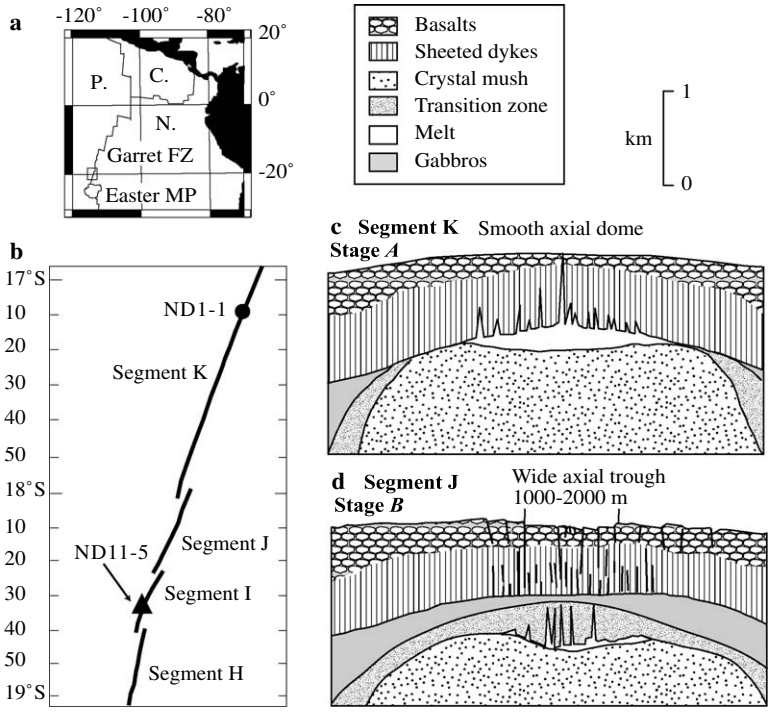

Fig. 5. The East Pacific Rise between 17° and 19 °S. (a) Location of the studied area along the southern East Pacific Rise. The two main ridge-axis discontinuities are indicated (FZ for fracture zone and MP for microplate). Abbreviations P., C., and N. are used for Pacific, Cocos and Nazca plates, respectively. (b) Synthetic map of the studied area with position of the four segments K, J, I, and H. Position of the two samples used in the geochemical application are reported. (c and d) Interpretative cross-sections of the ridge axial structure for typically smooth and notched segments, respectively. They show the connection between the time-related morphological evolution of the axial profile and the melt lens state. Modified after Hooft et al. (1997) and Lagabrielle and Cormier (1999).

Within the broad dome-shaped sections of the EPR, AMC width and depth vary systematically as a function of axial morphology and depth (Carbotte et al., 1997; Lagabrielle and Cormier, 1999). Where the AMC reflector is shallow and continuous over a long distance, the axial crest is devoid of any significant trough (smooth portions). In contrast, large troughs (500–2000 m wide and 20–100 m deep) occur, more rarely, at the axial dome summits beneath which short-wave variations in AMC reflector are observed (notched portions) (Lagabrielle and Cormier, 1999; Garel et al., 2002).

From the conclusions of Hooft et al. (1997) and Lagabrielle and Cormier (1999), a cyclic model can be proposed to account for the temporal evolution of the dome-shaped axis within the considered zone. It is based on three concepts: (i) it requires a composite magma chamber including a thin melt lens overlying a zone of crystal mush surrounded by a transition zone of mostly solidified crust (Sinton and Detrick, 1992) (Fig. 5c and d); (ii) the formation of large summit troughs is closely related to changes in the underlying reservoir, as is also suggested by other authors (e.g., Macdonald and Fox, 1988); and (iii) each axial morphology type corresponds to a time-related evolutionary stage of a given portion of the ridge. A smooth morphology (segment K type) corresponds to a robust magma supply to the lens (stage *A*: Fig. 5c). When magma supply begins to decrease, faults appear through the thin brittle crust, leading to changes in the thermal structure and to sinking of the magma lens. Concomitant, continuous magma expulsion/crystallization induces the progressive waning of the lens (stage *B*: Fig. 5d). The return to a strong replenishment stage produces rise and inflation of the magma lens. Among the EPR portions where the presence of an AMC is predicted with at least 75% confidence, one third is represented by notched segments (estimated from the Fig. 1 of Lagabrielle and Cormier, 1999). Given the connection between axial morphology and time, the relative duration of stages *A* and *B* can be estimated from their respective spatial extent. Thus, the duration of stage *B* should represent one third of a cycle period.

3.2. Geochemical data

Within the latitude interval corresponding to segments H, I, J, and K, the EPR portion between 17°S and 19°S has been intensively studied from a geological/geophysical point of view. The magmatic segments have also been characterized from major element and compatible trace element studies (Sinton et al., 1991; Mahoney et al., 1994). Moreover, incompatible trace element data on fresh and recent samples are available along the considered axial zone. In our modeling, only rare earth elements (REE) measured on N-MORB have been considered. Our set includes the 31 data from Caroff et al. (1997), combined with ten

analyses from the PETDB (petrological database of the ocean floor) electronic database (Kay et al., 1970; Hékinian et al., 1995; Niu et al., 1996; see www.petdb.org). This set may be considered representative of the compositional variability of the lavas in the studied ridge portion, even if the geochemical differences between the segments are possibly attenuated due to the involvement of a few older samples resulting from a previous stage of the magma system evolution. La and Er, which display more scattered variations than their neighboring REE, are shown in Fig. 6a, but not included in the quantitative modeling.

The chondrite-normalized REE patterns are broadly parallel and show a depletion in light REE for all segments (Fig. 6a). Moreover, these patterns corroborate the observations made by Batiza et al. (1995) from major element studies: samples from segments H, I, and J are more compositionally heterogeneous than samples from segment K, and they include the most differentiated lavas (Fig. 6). The compositional differences observed between N-MORB from segment K and those from segments H, I, and J are not due to mantle source heterogeneities, because the highly incompatible trace element ratios and the Sr, Nd, and Pb isotopic ratios remain constant along the EPR axis between 17°S and 19°S (e.g., Niu et al., 1996). Thus, only variations in the extent of partial melting and/or fractional crystallization could explain such a chemical diversity.

Helium and neon isotopes measured on EPR lavas between 13° and 23°S are variable, but not correlated with other isotopes, major elements, and trace elements. This feature argues against large differences in the degree of melting or depth of melting (Kurz et al., 2005). Using the inverse method of Maaløe (1994), we have tested the geochemical consequences on lava compositions of an increase of the partial melting degree from 17% to 20%, a range proposed for this zone by Bach et al. (1994). Although non negligible, this process can only account for less than 20% of the total amplitude observed for REE variations.

3.3. Model parameters

Some input parameters need to be constrained using geophysical and geological observations prior to applying the model on a natural site. Given the relative constancy of MORB densities in a large range of compositions (Sparks et al., 1980), melt quantities can be equally expressed as masses or as volumes. In the case of EPR 17–19°S, we have chosen as input parameters (Table 1):

- $\overline{q}_i$ (expressed as mean volume of magma injected in the reservoir for one year),
- $Q_A - Q_B$ (difference between the volume of resident magma at the end of stage A and at the end of stage B, i.e. amplitude of the Q function as expressed in Eq. (9)),
- r_e (mean ratio between rate of extrusion and rate of crystallization),

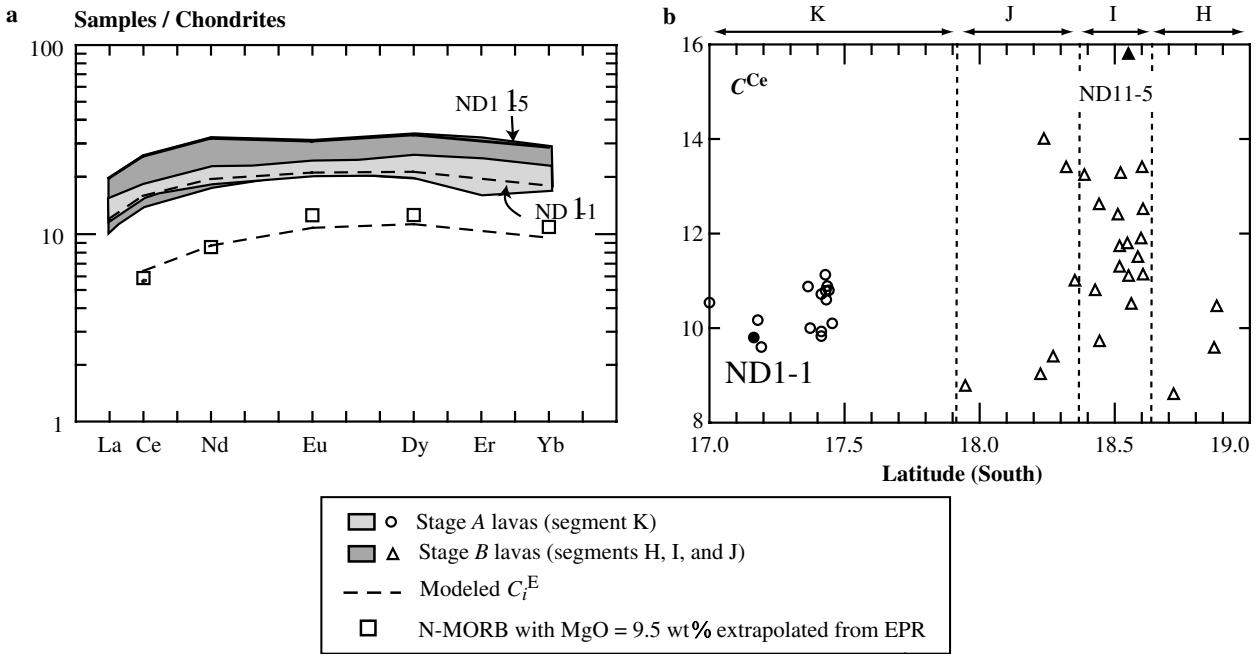

Fig. 6. Geochemical data on axial lavas collected from EPR 17–19°S (Kay et al., 1970; Hékinian et al., 1995; Niu et al., 1996; Caroff et al., 1997). (a) Chondrite-normalized REE diagram (normalization values from Sun and McDonough, 1989), with fields for lavas from stages A (smooth segment, 15 samples) and B (notched segments, 26 samples). Samples used for geochemical modeling are indicated (ND1-1 and ND11-5 for the most primitive and the most differentiated samples, respectively). The composition of intruded magma C_i^E is compared with the composition of a mafic MORB from EPR with MgO = 9.5 wt% (see text). The C_i^{REE} values have been calculated using the set of bulk distribution coefficients estimated by combining individual K_D with an appropriate crystallizing assemblage (D_2^{REE}). (b) Variations of Ce content with latitude. The compositional range of lavas erupted during stage A (segment K) is more restricted than that of stage B lavas (segments J, I, and H). Full symbols denote samples used for geochemical modeling.

- C^E (REE concentrations in lavas, regarded as representative of expelled liquids),
- and D^E (bulk distribution coefficient of the incompatible trace element E).

Volumes are defined for a 20 km-long ridge portion. This corresponds approximately to the length of a third order segment and may represent the area likely to be affected by a single eruptive event (Sinton et al., 2002).

To constrain the $\overline{q}_i$ value for a 20 km-long EPR portion, we have considered (after Hooft et al., 1997) that, provided that there is no strong along-axis magma transport at crustal levels, crustal thickness is the most direct estimation of ridge magma supply. Consequently, the $\overline{q}_i$ value along 20 km axis, for a 6.8 km-thick crust (White et al., 1992) and a spreading rate of 150 mm/yr, is 0.02 km^3 by year.

The $Q_A - Q_B$ value can be estimated from the maximum variation of the lens volume between stages A and B, without taking into account the distal parts of the lens where small volumes of fractionated magma might pond. We have considered a fully molten inflated lens 120 m thick, 1200 m wide, and 20 km long (stage A) (Hussenoeder et al., 1996; Collier and Singh, 1997; Carbotte et al., 2000) and an empty deflated one (stage B), which implies a volume difference of ca. 3 km^3. Assuming the constancy of the spreading rate, another way to approach this volume variation is to consider the maximum empty space created during the formation of the large summit trough. If we consider a 20 km-long axial trough 2 km wide and 110 m deep (Lagabrielle and Cormier, 1999), we obtain a volume of ca. 4.5 km^3. These values are rather similar, even if emptying a lens cannot account entirely for the formation of the summit depression. The slight difference could reflect the partial draining of the interstitial melt. Thus, calculations have been performed with a $Q_A - Q_B$ value equal to 4.5 km^3.

The ratio r_e can be written Q_e/Q_c if Q_e and Q_c are zero at the start of the process. We have approximated it using the ratio between the thickness of seismic layers 2 (basaltic lavas plus sheeted dykes: ca. 2 km) and 3 (gabbroic rocks: ca. 4.8 km), i.e. $r_e \sim 0.42$. We have used a r_e equal to 0.4, to account for the slight density contrast between basalts and gabbros.

The procedure also requires us to constrain the range of REE concentrations in the erupted magmas, i.e. the minimum and maximum REE concentrations in the lavas. We have selected two rocks representative of the extreme compositions of our set: ND1-1, the most depleted sample for the REE taken as a whole, and ND11-5 (Caroff et al., 1997) (Table 2 and Fig. 6).

A first set of bulk REE distribution coefficients (D_1) has been calculated from the chemical data, except for Ce which has been taken as the reference incompatible trace element. D_1^{Ce} has been arbitrarily fixed to 0.01. The other D_1 values have been estimated through the slope S in diagrams ln C^E *versus* ln C^{Ce}. For each REE, S has been calculated by least square linear regression: $D_1 = S(D_1^{Ce} - 1) + 1$. This approach assumes Rayleigh fractionation, which is hardly consistent with an open-system magma chamber. Consequently, we have calculated another set of bulk distribution coefficients (D_2) by combining individual mineral/liquid distribution coefficients (K_D from Fujimaki et al., 1984) with an appropriate crystallizing assemblage (approximately 10 wt% olivine, 35 wt% clinopyroxene, and 55 wt% plagioclase, L. Coogan pers. comm., 2005). The proportion of trapped melt cannot be estimated. Results are shown in Table 2. The fact that the two sets are significantly different will be used to test the robustness of the modeling.

4. Results

4.1. Geochemical approach

4.1.1. EPR 17–19°S

We have put into Eq. (12) the values of the input parameters r_e, D^E (calculated from two methods), and C^E discussed above. The two last unknown parameters, β and C_i^E, can be then estimated using a graphical method.

In Fig. 7 C^{Ce} is plotted against t which denotes a dimensionless time. Indeed, the time scale has no effect on the extreme C^{Ce} values as a result of the homogeneity of

Table 2
Lava samples used for the modeling on EPR 17–19°S and main results of the geochemical approach

	ND1-1	ND11-5	D_1	β (a)	C_i (a)	D_2	β (b)	C_i (b)	β (c)	C_i (c)
Segment shapes	Smooth	Notched								
Segments	K	I								
Latitude	17°09.93′S	18°33.28′S								
Ce	9.8	15.8	0.01	4.10	3.47	0.06	3.90	3.87	13.5	3.99
Nd	9.16	15	0.10	3.61	3.94	0.11	3.57	4.02	12.4	4.14
Eu	1.23	1.8	0.40	3.12	0.80	0.21	4.12	0.62	14.1	0.63
Dy	5.44	8.5	0.35	2.87	3.38	0.22	3.46	2.84	12.1	2.98
Yb	3.08	4.9	0.32	2.89	1.85	0.22	3.32	1.61	11.5	1.66
Mean				3.32			3.67		12.72	

REE compositions of samples ND1-1 and ND11-5 (from Caroff et al., 1997) are expressed in ppm (glasses analyzed by ICP-MS). The bulk distribution coefficients have been determined by two methods: by least square linear regressions from our sample set (D_1) and by combining individual K_D with a crystallizing assemblage (D_2): see text for more explanations. C_i (ppm) and β are the output parameters deduced from the geochemical model, for a equal to 0 km^3/(year.20 km ridge): (a) using the D_1 set; (b) using the D_2 set; and for a equal to 0.01 km^3/(year.20 km ridge), using the D_2 set: (c).

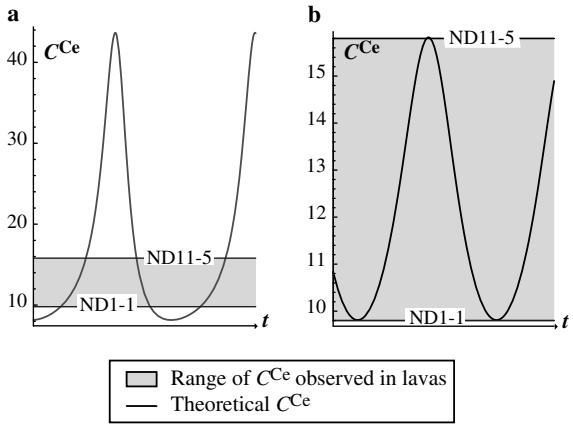

Fig. 7. Resolution procedure used to constrain C_i^{Ce} and β from the measured Ce concentrations plotted against dimensionless time. The evolution of C^{Ce} with time is calculated from Eq. (12), with $\omega = 1$, $r_e = 0.4$ and $D_1^{Ce} = 0.01$. The aim is to fit theoretical and analytical concentration ranges. (a) Curve position after adjustment of C_i^{Ce} (equal to 3.47 ppm) but with an unsuitable β value. The median of the curve is centered on the lava concentration range. (b) Curve position after adjustment of parameters C_i^{Ce} and β (equal to 4.10): theoretical and analytical concentrations now fit perfectly.

Eq. (12). The first step in the modeling fixes β and C_i^{Ce} arbitrarily. C_i^{Ce} is then adjusted until the calculated median C^{Ce} value is centered on the lava concentration range (Fig. 7a). Finally, β is adjusted to match the calculated and measured maximum and minimum concentrations (Fig. 7b). This procedure has been applied to the other REE. Results are shown in Table 2. The consistency of the D^{REE} coefficients can be tested from the reproducibility of the β values. They vary from 2.87 to 4.10 for the D_1 set (linear regression) and from 3.32 to 4.12 for the D_2 set (crystallizing assemblage). The two ranges of β values are rather restricted given the non linear property of this parameter. However, the D_2^{REE} values lead to less scattered β values (Table 2).

The C_i^{REE} values calculated from the two sets of D^{REE} are fairly similar (Table 2). The D_1 values merely lead to stronger LREE/HREE fractionation in C_i^{REE}. Given both the questionable method of calculation of D_1^{REE} and the more scattered corresponding β values, our preferred β and C_i^{REE} values will be henceforth those derived from experimental K_D values (D_2^{REE} set).

Our preferred C_i^{REE} values are shown in Fig. 6a together with the range of C^{REE} measured in lavas. Concentrations in the refilling melt are clearly lower than those in effusive rocks, a feature consistent with its primitive character. The C_i^{REE} pattern is grossly parallel to those of the lavas. We have calculated the REE *versus* MgO linear regressions with 186 N-MORB from EPR and then estimated the mean REE composition of an EPR lava with MgO = 9.5 wt% (Fig. 8), in order to check the geological significance of the C_i^{REE} set. The results, plotted in Fig. 6a, are close to the C_i^{REE} values. Such a primitive composition suggests that a magma which has previously undergone little differentiation and/or assimilation can be delivered to the axial reservoir. This result is consistent with a model in which most of

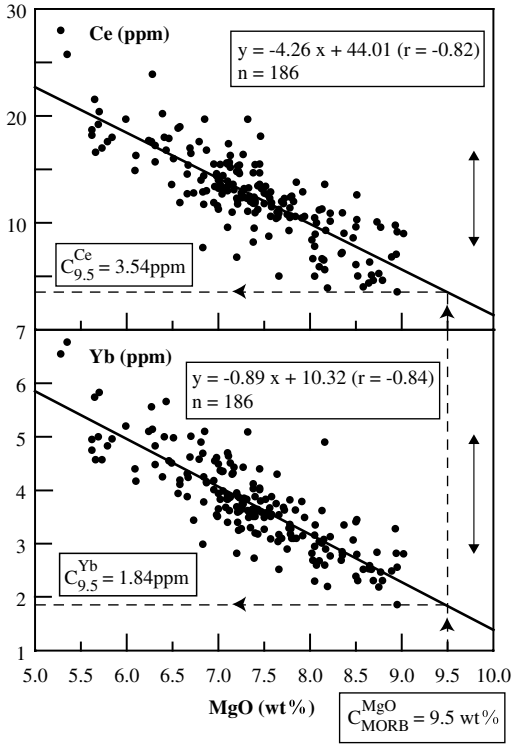

Fig. 8. Ce and Yb *versus* MgO diagrams for 186 N-MORB from EPR ($5 < MgO < 10$ wt%), compiled from the PETDB database. Linear regressions have been calculated for all the REE *versus* MgO diagrams. They are used to estimate the REE composition of an average MORB with a MgO content equal to 9.5 wt%. Arrows at the right side of the diagrams indicate the range of Ce and Yb variations for the data from 17°S to 19°S.

the crystal nucleation and growth processes occur within the AMC (Quick and Denlinger, 1993; Coogan et al., 2002).

4.1.2. NS-PSC 18–19°S

The north-south propagating spreading center from the North Fiji Basin (NS-PSC), located between 18°10′S and 20°50′S, propagates northwards at a rate of *c.* 57 mm/yr since at least 1 Ma. The N-MORB lavas from its northern dome-shaped segment, located between 18 and 19°S (NS-PSC 18–19°S), are characterized by homogeneous Sr and Nd isotopic ratios as well as nearly constant incompatible trace element ratios (Fleutelot et al., 2005). These data argue against mantle source heterogeneties. In addition, there is no evidence for occurrence of an assimilation process. Caroff and Fleutelot (2003) have suggested that magmas migrate through several open-system reservoirs along the propagating segment. In their view, at least the two most mafic lava groups (M1 and M2, Table 3) were erupted from cyclically replenished magma chambers, following the model of Albarède (1985). The composition of the fresh mafic liquid replenishing the reservoir (L0, Table 3), which is an input parameter in their model, has been estimated for mineralogical and geochemical data (Caroff and Fleutelot, 2003). The L0 liquid is periodically injected into a first magma chamber, which expels M1-type magmas both

Table 3
Lava samples used for the modeling on NS-PSC 18–19°S and main results of the geochemical approach

	M1	M2	D	β	C_i	L0
Y	31.1	40.6	0.2325	5.74	15.69	17.9
Zr	66	97	0.061	4.85	25.4	27
Nb	1.56	2.61	0.008	3.81	0.56	0.63
La	2.29	3.50	0.1215	4.11	1.01	1.07
Ce	7.79	11.71	0.0915	4.42	3.22	3.69
Nd	6.98	10.37	0.127	4.38	3.07	2.78
Eu	1.05	1.33	0.2655	6.20	0.55	0.52
Dy	5.18	6.74	0.2325	5.81	2.61	3.01
Er	3.15	4.10	0.2315	5.81	1.59	1.85
Yb	3.17	4.11	0.2355	5.87	1.60	1.84

M1 and M2 correspond to the average incompatible trace element compositions of lavas from group 1: 64 ⩾ mg# ⩾ 61 and lavas from group 2: 59 ⩾ mg# ⩾ 52, respectively (Caroff and Fleutelot, 2003, their Table 1). L0 is the parental liquid composition estimated by least square linear regression for a mg# value of 69 (Caroff and Fleutelot, 2003, their Table 1). M1, M2, and L0 are expressed in ppm. The D values correspond to the average values of the bulk distribution coefficients estimated by Caroff and Fleutelot (2003) for stages 1 and 2 in their Table 3. C_i (ppm) and β are the output parameters deduced from the geochemical model, with rates of crystallization and extrusion regarded as constant.

through the overlying crust and into another reservoir located closer to the northern extremity of the propagating spreading center. This second reservoir periodically expels M2-type liquids.

Given the apparent similarity between the magma system behavior in both oceanic ridge zones (EPR 17–19°S and NS-PSC 18–19°S), we have tested the geochemical formulation of our model on this second site. For that purpose, we have regarded the two interconnected reservoir as one single magmatic system, replenished by a L0-type mafic liquid and expelling both M1- and M2-type magmas. The parameter values put into Eq. (12) (Table 3) are: 0.4 for r_e, as in the EPR case; for D^E, the average values of the bulk distribution coefficients estimated by Caroff and Fleutelot (2003) for stages 1 and 2 (their Table 3); M1 and M2 as C^E_{min} and C^E_{max}, respectively. The output parameters, β and C^E_i, are also shown in Table 3. The β values ranges from 3.81 to 6.20 and the C^E_i and L0 values are very similar, with relative deviation values ranging from 5.6% (Eu) to 15.1% (Er). The fact that we find again the composition of the refilling liquid shows that simpler mass balance steady-state open-system models, such as those proposed by O'Hara (1977) and Albarède (1985), are not inconsistent with our approach. This result illustrates with natural data the kinship between the different models of periodically replenished reservoirs already shown above in the theoretical sections.

4.2. Extended approach

In the specific case of the EPR between 17° and 19°S, the available geological and geophysical data allow further modeling steps.

The mean β value calculated from the D_2^{REE} set (Table 2), together with the geological parameters $\overline{q}_i$ and r_e, are put into the amplitude $Q_A - Q_B$ of the Q function as expressed in Eq. (9):

$$Q_A - Q_B = \frac{2\overline{q}_i}{\alpha\sqrt{(1+r_e)^2+\beta^2}}. \quad (16)$$

It is then possible to calculate α, the melt fraction crystallized per time unit, from which the period $T = 2\pi/(\alpha\beta)$ can be determined. Then, all quantities are entirely constrained, either from Eq. (9) or by integrating Eqs. (2) and (3). It is therefore possible to determine some of their characteristics, such as the extreme volumes Q_A (maximum value) and Q_B (minimum value) of the resident magma. Assuming that the duration of stage B (notched morphology) represents one third of the cycle period during which the Q values are the lowest, it is possible to compute the total volumes of magmas crystallized (ΔQ_c) and ejected (ΔQ_e) during each stage.

The results of these calculations are shown in Table 4. The period, corresponding to the duration of stages A plus B, is 757 years, whereas the residence time is 316 years. By using the D_1 set (Table 2), the results are almost identical (period: 767 years and residence time: 290 years). The value of the residence time cannot be directly validated, because such a short time scale cannot be checked using most of the current isotopic methods. Only high resolution isotopic disequilibrium methods (e.g., $^{226}Ra/^{230}Th$) could give accurate temporal information, but very few data are available on the MORBs (e.g., Sims et al., 2002; Blake and Rogers, 2005) and the interpretation in terms of residence time is sometimes complex (e.g., Goldstein et al., 1999). Following Blake and Rogers (2005) who have studied magma differentiation rates from ($^{226}Ra/^{230}Th$) in several sites including

Table 4
Results of the extended approach on EPR 17–19°S

	km³/(year.20 km ridge)	$a = 0$	$a = 0.01$
T	year	757	711
α_p	year^{-1}	23×10^{-4}	7×10^{-4}
Q_B	km³/(20 km ridge)	4.1	3.92
Q_A	km³/(20 km ridge)	8.6	8.42
τ	year	316	308
Stage A: Smooth axial morphology			
ΔQ_c	km³/(20 km ridge)	8.27	7.08
$\Delta Q_c/(2T/3)$	km³/(year.20 km ridge)	0.017	0.015
ΔQ_e	km³/(20 km ridge)	3.31	2.83
$\Delta Q_e/(2T/3)$	km³/(year.20 km ridge)	0.007	0.006
Stage B: Notched axial morphology			
ΔQ_c	km³/(20 km ridge)	2.54	3.08
$\Delta Q_c/(T/3)$	km³/(year.20 km ridge)	0.010	0.013
ΔQ_e	km³/(20 km ridge)	1.02	1.23
$\Delta Q_e/(T/3)$	km³/(year.20 km ridge)	0.004	0.005

ΔQ_c, total volume of magma crystallized during a stage. ΔQ_e, total volume of magma ejected during a stage. To obtain the mean volumes of magma crystallized and ejected by year, ΔQ_c and ΔQ_e are divided by the postulated duration of stages A and B ($2T/3$ and $T/3$, respectively).

EPR 9–10°N, the time required to generate moderately evolved magmas (fraction of remaining liquid inferior to 0.7) is of the order of 500–1500 years. The resident time calculated here is also remarkably consistent with values proposed for open-system reservoirs feeding permanently active basaltic volcanoes (e.g., a few 10^2 to 10^3 years : West et al., 2001; Condomines et al., 2003). The crystallized fraction of magma is 23×10^{-4} year^{-1}. Blake and Rogers (2005) have calculated crystallization rate values ranging from 2×10^{-4} to 5×10^{-4} year^{-1} for EPR 9–10°N. As a comparison, Vigier et al. (1999) have proposed a value of ca. 3.5×10^{-4} year^{-1} for an equivalent parameter measured by U–Th disequilibria for the 1978 eruption of Ardoukoba, Asal Rift (Djibouti). The maximum amplitude of the reservoir drain corresponds to the difference between 8.6 and 4.1 km^3/(20 km ridge). Finally, the mean volumes of magma crystallized or expelled per year during stage *B* represent 61% of the corresponding volumes during stage *A* (Table 4).

4.3. Trends in the non-proportional model

The procedure described in Section 2.4 allows us to investigate the effects of variations in the rate of crystallization and extrusion. In order to highlight the trends induced by this more realistic approach, we show in Tables 2 and 4 the results obtained (using the D_2 set) for a high value of crystallized magma volume fixed independently of Q: $a = 0.01$ km^3/(year.20 km ridge). With such a positive a value, the fraction crystallized per unit time α increases when the reservoir size is decreasing. A negative a value would have an opposite effect.

For the chosen a value, 70% of the 0.02 km^3 injected by year which leave the system are independent of the reservoir size (50% crystallization and 20% extrusion for a r_e value equal to 0.4). Only the remaining 30% are proportional. The resolution method is similar to that presented in Section 4.1 and Section 4.2.

The differences between the results with $a = 0$ and $a = 0.01$ km^3/(year.20 km ridge) are not geologically significant. The C_i^{REE} values slightly increase (within the analytical error bar, Table 2), and the period decreases by ca. 6%, whereas the residence time remains similar. The crystallized and expelled volumes during stage *B* increase from 0.010 to 0.013 km^3/(year.20 km ridge) and from 0.004 to 0.005 km^3/(year.20 km ridge), respectively (Table 4). The differences between the results obtained using the two a values are too small to justify the use of such a complex approach.

5. Conclusions

The purpose of the theoretical treatment presented in this paper is to model the geochemical evolution of changing volume magma chambers, continuously replenished and tapped, whatever their geodynamic settings. We have used a sinusoidal function in order to model magma input, but other kinds of replenishment might be evaluated, even non-continuous input functions (provided that the practical application is adapted).

The use of the sinusoidal model requires a rather good knowledge of the geological setting together with the extreme values of the lava compositional range. A first step can be used to calculate the incompatible trace element composition of the replenishment liquid. If additional geological data are available, it is possible to evaluate other parameters such as period, residence time, reservoir sizes, crystallized and expelled volumes.

The geochemical formulation of this model has been tested on the north-south propagating spreading center located in the North Fiji Basin between 18°S and 19°S. The calculated composition of refilling liquid is almost similar to that previously estimated from experimental data.

The model has been applied to the East Pacific Ridge between 17°S and 19°S, an intensively studied region known for its strong magma budget. Our calculations suggest a periodic refilling of the chamber by a rather Mg-rich MORB magma (MgO = 9.5 wt%), a magma residence time of ca. 300 years and a cycle period of ca. 750 years.

Acknowledgments

We thanks M.-H. Cormier for her useful comments on the geological parameters and R. Merle for his pioneering work in this study. Detailed and constructive comments by Drs. W.A. Bohrson, L.A. Coogan, M. Jellinek, J. Pietruszka, and four anonymous reviewers helped us to improve the manuscript. We also thank Dr. R.C. Maury for his judicious suggestions as well as Drs. F.A. Podosek, F.A. Frey, and K.J. Russel for their editorial assistance. Contribution no.1007 of the IUEM, European Institut for Marine Studies (Brest, France).

Associate editor: Frederick A. Frey

References

Albarède, F., 1985. Regime and trace-element evolution of open magma chambers. *Nature* **318**, 356–358.

Albarède, F., 1993. Residence time analysis of geochemical fluctuations in volcanic series. *Geochim. Cosmochim. Acta* **57**, 615–621.

Auzende, J.-M., Ballu, V., Batiza, R., Bideau, D., Charlou, J.L., Cormier, M.H., Fouquet, Y., Geistdoerfer, P., Lagabrielle, Y., Sinton, J., Spadea, P., 1996. Recent tectonic, magmatic and hydrothermal activity on the East Pacific Rise between 17°S and 19°S: submersible observations. *J. Geophys. Res.* **101**, 17995–18010.

Bach, W., Hegner, E., Erzinger, J., Satir, M., 1994. Chemical and isotopic variations along the superfast spreading east Pacific Rise from 6 to 30°S. *Contrib. Mineral. Petrol.* **116**, 365–380.

Batiza, R., Bideau, D., Sinton, J.M., Spadea, P., 1995. Basalt varitions at super-fast spreading East Pacific Rise, 17–19°S (Naudur cruise). *Terra Abstr.* **7**, 145, abstr.

Blake, S., Rogers, N., 2005. Magma differentiation rates (^{226}Ra/^{230}Th) and the size and power output of magma chambers. *Earth Planet Sci. Lett.* **236**, 654–669.

Carbotte, S., Mutter, J.C., Xu, L., 1997. Contribution of volcanism and tectonism to axial flank morphology of the southern East Pacific Rise,

17°10′–17°40′S, from a study of layer 2A geometry. *J. Geophys. Res.* **102**, 10165–10184.

Carbotte, S.M., Solomon, A., Ponce-Correa, G., 2000. Evaluation of morphological indicators of magma supply and segmentation from a seismic reflection study of the East Pacific Rise 15°30′–17°N. *J. Geophys. Res.* **105**, 2737–2759.

Caroff, M., Fleutelot, C., 2003. The north-south propagating spreading center of the North Fiji Basin. Modeling of the geochemical evolution in periodically replenished and tapped magma chambers. *Mineral. Petrol.* **79**, 203–224.

Caroff, M., Lagabrielle, Y., Spadea, P., Auzende, J.-M., 1997. Geochemical modeling of nonsteady-state magma chambers: a case study from an ultrafast spreading ridge, East Pacific Rise, 17–19°S. *Geochim. Cosmochim. Acta* **61**, 4367–4374.

Cioni, R., Civetta, L., Marianelli, P., Metrich, N., Santacroce, R., Sbrana, A., 1995. Compositional layering and Syn-eruptive mixing of a periodically refilled shallow magma chamber: the AD 79 plinian eruption of vesuvius. *J. Petrol.* **36**, 739–776.

Collier, J.S., Singh, S.C., 1997. Detailed structure of the top of the melt body beneath the East Pacific Rise at 9°40′N from waveform inversion of seismic reflection data. *J. Geophys. Res.* **102**, 20287–20302.

Condomines, M., Gauthier P.-J., Sigmarsson, O.R., 2003. Timescales of magma chamber processes and dating of young volcanic rocks. In: Bourdon, B., Henderson, G.M., Lundstrom, C.C., Turner, S.P. (Eds.), *Uranium-series Geochemistry*, vol. 52,. Review in Mineralogy and Geochemistry, Washington, DC, pp. 125–174.

Coogan, L.A., Thompson, G., MacLeod, C.J., 2002. A textural and geochemical investigation of high level gabbros from the Oman ophiolite: implications for the role of the axial magma chamber at fast-spreading ridges. *Lithos* **63**, 67–82.

De Paolo, D.J., 1981. Trace element and isotopic effects of combined wallrock assimilation and fractional crystallization. *Earth Planet Sci. Lett.* **53**, 189–202.

DeMets, C., Gordon, R.G., Argus, D.F., Stein, S., 1990. Current plate motions. *Geophys. J. Int.* **101**, 425–478.

Detrick, R.S., Buhl, P., Vera, E.E., Mutter, J.C., Orcutt, J.A., Madsen, J.A., Brocher, T.M., 1987. Multichannel seismic imaging of a crustal magma chamber along the East Pacific Rise. *Nature* **326**, 35–41.

Edwards, B.R., Russell, J.K., 1998. Time scales of magmatic processes: new insights from dynamic models for magmatic assimilation. *Geology* **26**, 1103–1106.

Fleutelot, C., Eissen, J.-P., Dosso, L., Juteau, T., Launeau, P., Bollinger, C., Cotten, J., Danyushevsky, L., Savoyant, L., 2005. Petrogenetic variability along the North-South Propagating Spreading Center of the North Fiji Basin. *Mineral. Petrol.* **83**, 55–86.

Fujimaki, H., Tatsumoto, M., Aoki, K.-I., 1984. Partition coefficients of Hf, Zr, and REE between phenocrysts and groundmasses. *J. Geophys. Res.* **89**, 662–672.

Garel, E., Dauteuil, O., Lagabrielle, Y., 2002. Deformation processes at fast to ultra-fast oceanic spreading axes: mechanical approach. *Tectonophysics* **346**, 223–246.

Ghiorso, M.S., Sack, R.O., 1995. Chemical mass transfer in magmatic processes: IV. A revised and internally consistent thermodynamic model for the interpolation and extrapolation of liquid-solid equilibria in magmatic systems at elevated temperatures and pressures. *Contrib. Mineral. Petrol.* **119**, 197–212.

Gillis, K.M., Coogan, L.A., 2002. Anatectic migmatites from the roof of an ocean ridge magma chamber. *J. Petrol.* **43**, 2075–2095.

Goldstein, S.J., Sims, K.W.W., Murrell, M.T., Nunn A.J., 1999. Evidence for radium–barium fractionation in MORB plagioclase: implication for geochronology and mantle melting. In: *Implications for Geochronology and Mantle Melting*, 9th Annual V.M. Goldschmidt Conference, Boston, MA, August 22–27 (abstr.).

Hawkesworth, C.J., Blake, S., Evans, P., Hughes, R., Macdonald, R., Thomas, L.E., Turner, S.P., Zellmer, G., 2000. Time scales of crystal fractionation in magma chambers—integrating physical, isotopic and geochemical perspectives. *J. Petrol.* **41**, 991–1006.

Hékinian, R., Bideau, D., Hébert, R., Niu, Y., 1995. Magmatism in the Garrett transform fault (East Pacific Rise near 13°27′S). *J. Geophys. Res.* **100**, 10163–10185.

Hooft, E.E.E., Detrick, R.S., Kent, G.M., 1997. Seismic structure and indicators of magma budget along the Southern East Pacific Rise. *J. Geophys. Res.* **102**, 27319–27340.

Humler, E., Whitechurch, H., 1988. Petrology of basalts from the Central Indian Ridge (lat. 25°23′S, long. 70°04′E): estimates of frequencies and fractional volumes of magma injections in a two-layered reservoir. *Earth Planet. Sci. Lett.* **88**, 169–181.

Hussenoeder, S.A., Collins, J.A., Kent, G.M., Detrick, R.S., 1996. Seismic analysis of the axial magma chamber reflector along the southern East Pacific Rise from conventional reflection profiling. *J. Geophys. Res.* **101**, 22087–22105.

Hussenoeder, S.A., Detrick, R.S., Kent, G.M., Schouten, H., Harding, A.J., 2002. Fine scale seismic structure of young upper crust at 17°20′S on the fast spreading East Pacific Rise. *J. Geophys. Res.* **107**. doi:10.1029/2001JB00168.

Kabeto, K., Sawada, Y., Iizumi, S., Wakatsuki, T., 2001. Mantle sources and magma-crust interactions in volcanic rocks from the northern Kenya rift: geochemical evidence. *Lithos* **56**, 111–139.

Kay, R., Hubbard, N.J., Gast, P.W., 1970. Chemical characteristics and origin of oceanic ridge volcanic rocks. *J. Geophys. Res.* **75**, 1585–1613.

Komor, S.C., Elthon, D., Casey, J.F., 1985. Mineralogic variation in a layered ultramafic cumulate at the North Arm Mountain Massif, Bay of Islands Ophiolite, Newfoundland. *J. Geophys. Res.* **90**, 7705–7736.

Kurz, M.D., Moreira, M., Curtice, J., Lott, D.E., Mahoney, J.J., Sinton, J.M., 2005. Correlated helium, neon, and melt production on the super-fast spreading East Pacific Rise near 17°S. *Earth Planet. Sci. Lett.* **232**, 125–142.

Lagabrielle, Y., Cormier, M.-H., 1999. Formation of large summit troughs along the East Pacific Rise as collapse calderas: an evolutionary model. *J. Geophys. Res.* **104**, 12971–12988.

Macdonald, K.C., Fox, P.J., 1988. The axial summit graben and cross-sectional shape of the East Pacific Rise as indicators of axial magma chambers and recent volcanic eruptions. *Earth Planet. Sci. Lett.* **88**, 119–131.

Maaløe, S., 1994. Estimation of the degree of partial melting using concentration ratios. *Geochim. Cosmochim. Acta* **58**, 2519–2525.

Maaløe, S., 2002. Physical behavior of the plume source during intermittent eruptions of Hawaiian basalts. *Contrib. Mineral. Petrol.* **142**, 653–665.

Mahoney, J.J., Sinton, J.M., Kurz, M.D., Macdougall, J.D., Spencer, K.J., Lugmair, G.W., 1994. Isotope and trace element characteristics of a super-fast spreading ridge: East Pacific Rise, 13–23°S. *Earth Planet. Sci. Lett.* **121**, 173–193.

Niu, Y., Waggoner, D.G., Sinton, J.M., Mahoney, J.J., 1996. Mantle source heterogeneity and melting processes beneath seafloor spreading centers: the East Pacific Rise, 18°S–19°S. *J. Geophys. Res.* **101**, 27711–27733.

O'Hara, M.J., 1977. Geochemical evolution during fractional crystallization of a periodically refilled magma chamber. *Nature* **266**, 503–507.

O'Hara, M.J., Herzberg, C., 2002. Interpretation of trace element and isotopic features of basalts: relevance of field relations, petrology, major element data, phase equilibria, and magma chamber modeling in basalt petrogenesis. *Geochim. Cosmochim. Acta* **66**, 2167–2191.

Pallister, J.S., Hopson, C.A., 1981. Samail Ophiolite plutonic suite: field relations, phase variation, cryptic variation and layering, and a model of a spreading ridge magma chamber. *J. Geophys. Res.* **86**, 2593–2644.

Quick, J.E., Denlinger, R.P., 1993. Ductile deformation and the origin of layered gabbro in ophiolites. *J. Geophys. Res.* **98**, 14015–14027.

Rabinowicz, M., Genthon, P., Ceuleneer, G., Hillairet, M., 2001. Compaction in a mantle mush with high melt concentrations and generation of magma chambers. *Earth Planet Sci. Lett.* **188**, 313–328.

Reagan, M.K., Gill, J.B., Malavassi, E., Garcia, M.O., 1987. Changes in magma composition at Arenal volcano, Costa Rica, 1968–1985: real-time monitoring of open-system differentiation. *Bull. Volcanol.* **49**, 415–434.

Scott, D.R., Stevenson, D.J., 1984. Magma solitons. *Geophys. Res. Lett.* **11**, 1161–1164.

Sims, K.W.W., Goldstein, S.J., Blichert-Toft, J., Perfitt, M.R., Kelemen, P., Fornari, D.J., Michael, P., Murrell, M.T., Hart, S.R., DePaolo, D.J., Layne, G., Ball, L., Jull, M., Bender, J., 2002. Chemical constraints on the generation and transport of magma beneath the East Pacific Rise. *Geochim. Cosmochim. Acta* **66**, 3481–3504.

Sinton, J.M., Detrick, R.S., 1992. Mid-ocean ridge magma chambers. *J. Geophys. Res.* **97**, 197–216.

Sinton, J.M., Smaglik, S.M., Mahoney, J.J., Macdonald, K.C., 1991. Magmatic processes at the superfast spreading mid-ocean ridges: glass compositional variations along the East Pacific Rise 13°–23°S. *J. Geophys. Res.* **96**, 6133–6136.

Sinton, J.M., Bergmanis, E.C., Rubin, K.H., Batiza, R., Gregg, T.K.P., Grönvold, K., Macdonald, K.C., White, S.M., 2002. Volcanic eruptions on mid-ocean ridges: new evidence from the superfast spreading East Pacific Rise, 17°–19 °S. *J. Geophys. Res.* **107**. doi:10.1029/2000JB00009.

Smewing, J.D., 1981. Mixing characteristics and compositional differences in mantle-derived melts beneath spreading axes: evidence from cyclically layered rocks in the ophiolite of north Oman. *J. Geophys. Res.* **86**, 2645–2659.

Sparks, R.S.J., Meyer, P., Sigurdsson, H., 1980. Density variation amongst mid-ocean ridge basalts: implications for magma mixing and the scarcity of primitive lavas. *Earth Planet. Sci. Lett.* **46**, 419–430.

Spera, F.J., Bohrson, W.A., 2002. Energy-constrained open-system magmatic processes III: energy-constrained recharge, assimilation and fractional crystallization (EC-RAFC). *Geochem. Geophys. Geosyst.* **3**. doi:10.1029/2002GC0031.

Spera, F.J., Bohrson, W.A., 2004. Open-system magma chamber evolution: an energy-constrained geochemical model incorporating the effects of concurrent eruption, recharge, variable assimilation and fractional crystallization (EC-E'RAχFC). *J. Petrol.* **45**, 2459–2480.

Sun, S.S., McDonough, W.F., 1989. Chemical and isotopic systematics of oceanic basalts: implication for mantle composition and processes. In: Saunders, A.D., Norry, M.J. (Eds.), *Magmatism in the Ocean Basins*, vol. 42. Geol. Soc. Spec. Pub., London, pp. 313–345.

Vigier, N., Bourdon, B., Joron, J.L., Allègre, C.J., 1999. U-decay series and trace element systematics in the 1978 eruption of Ardoukoba, Asal rift: timescale of magma crystallisation. *Earth Planet. Sci. Lett.* **174**, 81–97.

West, W., Menke, W., Tolstoy, M., Webb, S., Sohn, R., 2001. Magma storage beneath Axial volcano on the Juan de Fuca mi-ocean ridge. *Nature* **413**, 833–836.

White, R.S., McKenzie, D., O'Nions, R.K., 1992. Oceanic crustal thickness from seismic measurements and Rare Earth Elements inversions. *J. Geophys. Res.* **97**, 19683–19715.